A biocompatible redox MRI probe based on a Mn(ii)/Mn(iii) porphyrin

— **Source link** ↗

Sara M. A. Pinto, Mário J. F. Calvete, Mariana Emilia Ghica, Sergio Soler ...+9 more authors

Institutions: University of Coimbra, Autonomous University of Barcelona, University of Orléans

Related papers:

- Chemistry of MRI Contrast Agents: Current Challenges and New Frontiers

- Applications for Transition-Metal Chemistry in Contrast-Enhanced Magnetic Resonance Imaging

- Redox Cycling, pH Dependence, and Ligand Effects of Mn(III) in Oxalate Decarboxylase from Bacillus subtilis.

- Effects of cadmium on manganese peroxidase competitive inhibition of MnII oxidation and thermal stabilization of the enzyme.

- Quinol-containing ligands enable high superoxide dismutase activity by modulating coordination number, charge, oxidation states and stability of manganese complexes throughout redox cycling

Journal Name

ARTICLE

A Biocompatible Redox MRI Probe Based on a Mn(II)/Mn(III) Porphyrin

Sara M. A. Pinto[a,b,*], Mário J. F. Calvete[a,b], Mariana E. Ghica,[a] Sérgio Soler[c], Iluminada Gallardo[c], Agnès Pallier[d], Mariana B. Laranjo[b,e], Ana M.S. Cardoso[f], M. Margarida C. A. Castro[b,e], Christopher M.A. Brett,[a] Mariette M. Pereira,[a,b]*Éva Tóth[d,*] and Carlos F. G. C. Geraldes[b,e,*]

For the development of redox responsive MRI probes based on the Mn^{III}/Mn^{II} couple, stable complexation of both reduced and oxidized forms of the metal ion and appropriate tuning of the redox potential in the biologically relevant range are key elements. The water soluble fluorinated Mn-porphyrin derivative Mn-**3** satisfies both requirements. In aqueous solution, it can reversibly switch between Mn^{III}/Mn^{II} oxidation states. In the presence of ascorbic acid or β-mercaptoethanol, the Mn^{III} form undergoes reduction, which is fully reversed in the presence of oxygen. A UV-Vis kinetic study of Mn^{III}/Mn^{II} reduction yielded second-order rate constants, k_2, of 46.1 M^{-1} s^{-1} and 13.8 M^{-1} s^{-1} for the reaction with ascorbic acid and β-mercaptoethanol, respectively. This could correspond to a half-life of a few minutes in blood plasma and a few seconds in circulating immune cells where ascorbic acid reaches 20-40 μM and a few mM concentrations, respectively. Contrary to expectations based on the redox potential, reduction with glutathione or cysteine does not occur. It is prevented by the coordination of the glutathione carboxylate group(s) to Mn^{III} in axial position, as it was evidenced by NMR data. Therefore, Mn^{III}-**3** acts as an ascorbate specific turn-on MRI probe, which in turn can be re-oxydized by oxygen. The relaxivity increase from the oxidized to the reduced form is considerably improved at medium frequencies (up to 80 MHz) with respect to the previously studied Mn-TPPS$_4$ analogues; at 20 MHz, it amounts to 150%. No *in vitro* cytotoxicity is detectable for Mn-**3** in the typical MRI imaging concentration range. Finally, ^{19}F NMR resonances of Mn^{III}-**3** are relatively sharp which could open further opportunities to exploit such complexes as paramagnetic ^{19}F NMR probes.

Introduction

[a.] Department of Chemistry, Faculty of Science and Technology, University of Coimbra, Rua Larga, 3004-535, Coimbra, Portugal
[b.] Coimbra Chemistry Centre, CQC, University of Coimbra, Rua Larga, 3004-535, Coimbra, Portugal
[c.] Departament de Química, Universitat Autònoma de Barcelona, 08193 Bellaterra, Barcelona, Spain
[d.] Centre de Biophysique Moléculaire, CNRS, UPR 4301, Université d'Orléans, Orléans, France
[e.] Department of Life Sciences, Faculty of Science and Technology, University of Coimbra, Calçada Martim de Freitas, 3000-393, Coimbra, Portugal
[f.] Center of Neurosciences and Cell Biology, CNC, University of Coimbra, Rua Larga, Faculty of Medicine, 3004-504, Coimbra, Portugal
*Corresponding authors: C.F.G.C. Geraldes: geraldes@ci.uc.pt; E. Tóth: Eva .JAKABTOTH@cnrs.fr; S.M.A.Pinto: smpinto@qui.uc.pt

In any living body, both extracellular and intracellular redox environments are tightly regulated[1-3] and their dysregulation may be associated with a wide range of pathophysiological conditions, including chronic inflammation,[4] neoplastic growth[5] and ischemia,[6] since several triggered biochemical cascade events can damage cellular or tissue components, promoting disease progression.[7-9] The redox environment in a biological fluid, organelle, cell, or tissue is maintained by a number of redox couples present which are linked to each other. Among these, glutathione (GSH) is the major thiol-disulfide redox buffer of the cell with an average concentration of 1–11 mM in the cytosol, much higher than most other redox active compounds.[10] Therefore, the redox state of the glutathione disulfide-glutathione couple (GSSG/2GSH) can serve as an indicator of the intracellular redox environment. Changes of the half-cell reduction potential (E_{hc}) of the GSSG/2GSH couple appear to correlate with the biological status of the cell: proliferation E_{hc} ~ -240 mV; differentiation E_{hc} ~ - 200 mV; or apoptosis E_{hc} ~ -170 mV.[10] The extracellular space is typically more oxidized than the cytosol. In cell extracts, the total concentration of reduced (GSH) and oxidized (GSSG) glutathione present can be assessed by HPLC or fluorescent assays.[11, 12]

The development of imaging techniques capable of following *in vivo* tissue redox environment/activity is of utmost interest in clinical research and medical practice, particularly in diagnosis,

prognosis or monitoring therapeutic response.[13, 14] The fundamental goal of developing molecular probes capable of imaging redox activity has seen some clinical success. In particular, positron emission tomography (PET) probes capable of targeting hypoxic tissue, such as the radiotracers $^{64}Cu^{II}$-diacetyl-bis(N4-methylthiosemi-carbazone) ($^{64}Cu^{II}$-ATSM) and ^{18}F-fluoro-misonidazole (^{18}F-MISO), showed capacity to predict treatment outcome in patients undergoing radiotherapy.[15-17] The same hypoxia targeting mechanism of probe uptake (irreversible reaction and retention in oxygen-deprived tissue) has been extended to MRI contrast agents and fluorescent probes for optical imaging.[18, 19] Redox-sensitive nitroxide derivative probes were also used in electron paramagnetic resonance (EPR) imaging and spectroscopy to detect reductive environment (thiols and other reducing species).[20, 21]

Magnetic resonance imaging (MRI) is an attractive modality to monitor redox dynamics thanks to its exceptional spatial resolution (<100 μm using modern high-field equipment), lack of invasiveness and use of ionizing radiation, and its ability to simultaneously report physiological and anatomical information. Not surprisingly, the interest in the development of redox sensitive MRI probes has grown over the last years.[14, 22-26] These can be based on redox active ligands, undergoing a change in the ligand structure or the molecular rotation upon reduction/oxidation, while the oxidation state of the paramagnetic metal remains the same (*e.g.* merocyanine unit linked to a GdDO3A which isomerizes to the spirooxazine derivative by the redox stimulus of NADH).[27] Alternatively, complexes of redox active paramagnetic metals, like europium and manganese, can be also explored, in which the different oxidation states have different magnetic properties.[11, 22] Utterly, both types of probes must fulfill several requirements: i) biocompatibility, ii) a redox half-cell potential which is compatible with the redox potential of biological reducing agents; iii) strong signal change, if possible signal increase upon activation ("turn-on" probe); and iv) rapid redox kinetics as compared to the imaging time scale. Importantly, the redox active metal ion needs to be complexed by a ligand that is capable of efficiently chelating both oxidation states such that reduction or oxidation does not result in the decomposition of the complex.

Among redox active metal ions, manganese is particularly attractive for the development of redox responsive MRI probes, whose efficiency is measured by their proton relaxivity r_i ($i = 1,2$) (paramagnetic enhancement of the water proton relaxation rates, $R_i = T_i^{-1}$, where T_1 and T_2 are, respectively, the longitudinal and transverse relaxation times, referred to 1 mM concentration of the paramagnetic ion). Manganese is a biogenic element and in its +2 oxidation state, Mn^{2+}, is a very efficient paramagnetic relaxation agent. Mn^{2+} (d^5 configuration, high spin $S = 5/2$), with long (in the $0.1 - 1$ ns range) longitudinal electronic relaxation times and labile water exchange, is an attractive alternative to Gd^{3+} in MRI probes.[28, 29] Indeed, in the last years, there has been intensive research to identify suitable

ligand structures for Mn^{2+} chelation.[30, 31] Mn^{3+} (d^4 configuration) is also paramagnetic, usually giving rise to high spin $S = 2$ compounds. While water exchange is also fast,[14] the longitudinal electronic relaxation times are shorter (≤ 10 ps), making them less efficient relaxation agents.[32] The nuclear relaxation mechanism of Mn^{3+} is different from that of Mn^{2+} and therefore their relaxation efficiency shows a very distinct dependence on the external magnetic field B_0. While for the $S = 5/2$ Mn^{2+} complexes, the classical Solomon-Bloembergen-Morgan (SBM) formalism describes well nuclear relaxation, leading to a decrease of r_1 at high field, for the $S = 2$ Mn^{3+} complexes the analysis of the water proton relaxation rates is much less straightforward. Water soluble and air stable Mn^{3+}-porphyrins have been investigated as tumor targeted MRI agents.[33] For these compounds, the electron relaxation times are relatively long due to their higher symmetry.[32] For instance, the Mn^{III}-TPPS$_4$ (meso-tetra(4-sulfonatophenyl)porphine chloride) chelate[34] displays an anomalous r_1 relaxivity, with a peak above approximately 2 MHz. It was shown that the NMR relaxation mechanism has several unique aspects, including the unusual role of large rhombic zero-field splitting (ZFS) interactions, which are of the order of the nuclear Zeeman energy. The effect of these interactions on the electron spin dynamics leads to those relaxivity anomalies at high field.[35,36] As a consequence of the different relaxation mechanisms, the proton relaxivity, and thus the MRI efficiency can be either higher or lower for the reduced Mn^{2+} relative to the oxidized Mn^{3+} form, depending on the external magnetic field and on the chelating ligand.

Porphyrins, which are macrocyclic ligands *per excellence* and widely used in a multitude of applications, such as catalysis,[37-39] materials science[40-43] and biomedicine, including MRI,[30, 44-48] offer the possibility to obtain very stable chelates to host many metal ions, including paramagnetic ones. Such metalloporphyrins having a much reduced risk of transmetallation, may avoid potential *in vivo* metal release during the MRI examination which would cause toxicity, such as for instance gadolinium induced fibrosis disorders,[49] or manganese induced neurotoxicity.[50 50 50 50 50 50 50 50 50 50] Many studies have been reported of Mn^{III}-porphyrin dimers, supramolecular and macromolecular conjugates as MRI contrast agents,[33, 51-58] including enzyme[55, 56] and Zn^{2+}-responsive[57, 58] agents. So far, the only studies on Mn-porphyrins as redox MRI probes were reported by Aime and collaborators,[59] who explored a Mn^{II}/Mn^{III}-based water-soluble porphyrin (TPPS$_4$) as an oxygen sensor. However, at clinically relevant fields (^1H frequencies of 60-120 MHz), and at 25 ºC, the r_1 relaxivity values revealed to be very close for the Mn^{II} and Mn^{III} analogues. On the other hand, the formation of macromolecular conjugates, through the encapsulation of the Mn^{II}-TPPS$_4$ and Mn^{III}-TPPS$_4$ complexes in commercially available, water-soluble poly-β-cyclodextrin (CD), led to a marked difference in relaxivity at 20 MHz between the reduced and oxidized state.

Caravan and collaborators[30] explored hydroxybenzylethylenediamine acetic acid derivatives for Mn$^{II/III}$-chelation to create redox active contrast agents. The stability of the complexes was recently improved by using a "Janus" ligand that readily isomerizes between binding modes that favor either the Mn^{3+} or Mn^{2+} ion.[30] Rapid and reversible interconversion between the two oxidation modes was achieved by peroxidase activity (oxidation) and L-cysteine (reduction), which was translated into an unprecedented 9-fold relaxivity increase between the Mn^{3+} and Mn^{2+} analogue, respectively. One concern, nevertheless, about these open-chain complexes is the lack of a sufficiently high kinetic inertness which is desirable for *in vivo* applications.

Based on previous experience in porphyrin chemistry, our objective is to develop water soluble, biocompatible Mn-porphyrin complexes with a redox potential that is adapted to biological requirements. The approach to the development of such specifically designed Mn$^{II/III}$ complexes consists of modulating the redox potential by using appropriate electron withdrawing substituents on the porphyrin structure. The fine-tuning of the redox potential would be highly important since most of the redox responsive MRI probes reported so far do not undergo redox chemistry in a biologically relevant range.[22] The

capacity of porphyrin complexes to selectively localize in tumor cells is well known and will be a great advantage. Indeed, it can simplify probe design as no additional targeting and cell internalizing moieties are required, although they might be later added to the chemical structure to further improve these properties.

Herein we report the synthesis and physical-chemical characterization of a new fluorinated Mn$^{II/III}$ porphyrin derivative which was conjugated with PEG chains for better solubility and biocompatibility. Its redox properties were studied by cyclic voltammetry. The Mn^{III} reduction kinetics was followed in the presence of ascorbic acid and β-mercaptoethanol (BME) by UV-Vis. The relaxivity differences between the reduced and oxidized forms were investigated using ^{1}H Nuclear Magnetic Relaxation Dispersion (NMRD). Cytotoxicity evaluation of the system on epithelial HeLa cells is also reported.

Results and Discussion

Synthesis of the biocompatible porphyrin-based probes

The strategy adopted for the synthesis of the Mn^{III} biocompatible probe **3** is depicted in **Scheme 1**.
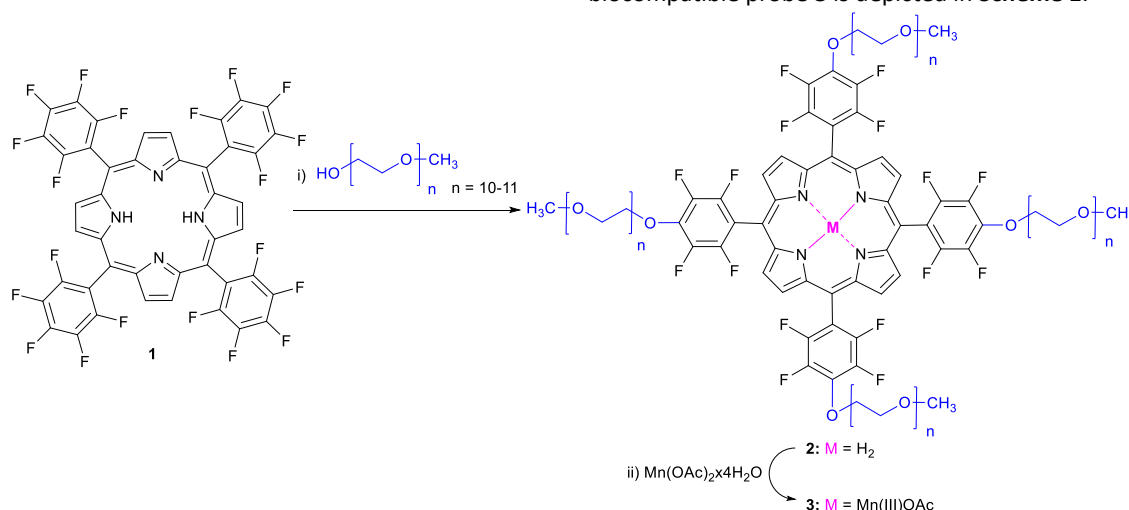
Scheme 1. Synthetic route for the preparation of the biocompatible porphyrin **3**. Reagents and conditions: i) DMF, NaH, room temperature, 2h; ii) acetic acid/sodium acetate, Mn(II)acetate tetrahydrate, 80ºC, 2h.

Porphyrin **1** was synthesized by the NaY method, developed by some of us,[60] where NaY acts as a reusable catalyst. After work-up 12% of the isolated porphyrin was obtained. In order to obtain free base porphyrin **2**, nucleophilic aromatic substitution of **1** using mono methyl protected polyethylene glycol with Mw = ~500 g/mol (PEG500) was performed, in DMF as solvent and NaH as base, at room temperature for two hours. The product was obtained in 65% yield, after purification, and fully characterized by ^{1}H, ^{19}F NMR spectroscopy and ESI-FIA-TOF

mass spectrometry (see **Figs. 1, S1, S2 and S3**, **ESI**). Its main characterization detailing feature was ascertained by observing the loss of the characteristic triplet (*p*-F) ^{19}F NMR signal at around -150 ppm (**Fig. 1**) for porphyrin **2**, when compared with the ^{19}F NMR spectrum of **1**, which presents its three typical (*m*-F), (*p*-F) and (*o*-F) signals at -160.2, -150.1 and -135.4 ppm, respectively (**Fig. 1**), confirming the tetrapegylation pattern obtained.
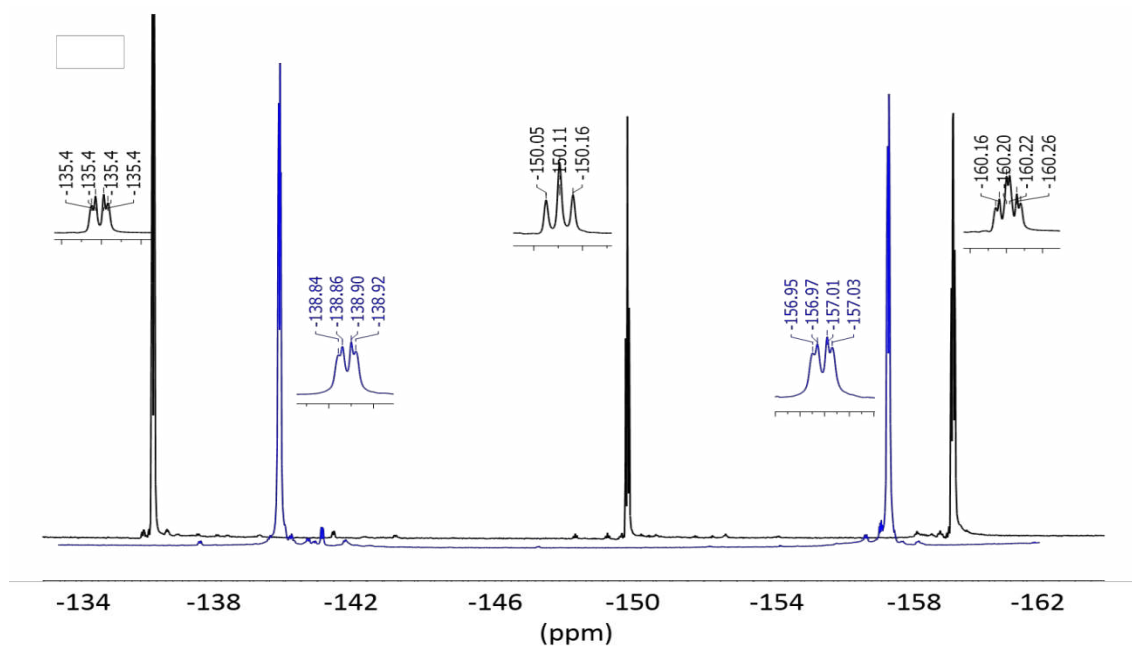
Journal Name

ARTICLE

Figure 1. ^{19}F NMR of porphyrin **1** (black spectrum) and porphyrin **2** (blue spectrum).

The preparation of Mn^{III}-**3** proceeded by reacting **2** with excess manganese diacetate tetrahydrate in sodium acetate/acetic acid buffer solution at 80 ºC for two hours. After several extractions of the crude with dichloromethane/water, the organic layer was dried with anhydrous sodium sulfate and concentrated under vacuum giving **3** in 82% yield (**Scheme 1**). The Mn^{III}-**3** complex was characterized by ESI-FIA-TOF mass spectrometry (see **Fig. S4, ESI**), presenting the characteristic poly-dispersed m/z peaks from PEGylated 1121.3612, 1319.9802, 1386.0195, 1493.6057 $[M]^{2+}$ (polydisperse distribution). Additionally, Electron Paramagnetic Resonance (EPR) experiments were also performed, in order to confirm the absence of the Mn^{II} salt used in the complexation reaction. The absence of the sharp sextet characteristic of the free aqueous Mn^{2+} cation even at a very high amplification, led to the conclusion that the Mn^{III}-**3** sample was free of aqueous Mn^{2+} (**Figure S5, ESI**).[47] The EPR spectrum of the Mn^{III}-**3** was also silent at room temperature, as expected from the fast electron relaxation characteristic of the integer-spin (non-Kramers) porphyrin compound.[61] Characteristic EPR resonances of Mn^{II}-porphyrins have been observed at liquid nitrogen temperature (e.g. a strong sextet at $g_\perp \sim 5.9$-5.2, a signal at $g_\parallel \sim 2.0$–2.1, and sometimes three other weak signals at 1.23, 0.77 and 0.54).[61,62] If some Mn^{II}-**3** were present in the sample, a broad signal at g_{iso} ~2.0 would be observable at room temperature,[62] which was not the case.

Proton and ^{19}F NMR

The proton NMR spectrum of Mn^{III}-**3** in $CDCl_3$ (**Fig. S6a**) shows a broad signal at -22.76 ppm corresponding to the β-pyrrole protons, characteristic of Mn^{III} high-spin *meso*-porphyrins. The large upfield shift and large broadening observed arise from the dominant contact mechanism, due to the small magnetic anisotropy of the coordinated Mn^{III} ion and consequent dipolar shift induced.[63, 64] The PEG chain CH_2 protons at 3.66 ppm are unshifted and hardly broadened relative to the signal at 3.65 ppm for free PEG due to their long distance from the paramagnetic center.

The ^{19}F NMR spectrum of Mn^{III}-**3** (**Fig. S6b**) consists of a broad signal centered at -126.2 ppm and a set of five upfield shifted (in the range of -149.7 to -157.7 ppm) sharper (linewidths around 190 Hz) signals of different intensities. This set of signals corresponds to the fluorine atoms at the *meta* positions of the *meso*-phenyl groups in the five possible combinations of the chain lengths of the four polydisperse PEG chains with n = 10-11. The broad signal around -126.2 ppm results from the overlap of the broader signals of the fluorine atoms at the ortho position, which are closer to the metal center.[65, 66] Upon reduction of Mn^{III}-**3** to Mn^{II}-**3**, all the ^{19}F resonances are completely broadened out, in accordance with the efficient paramagnetic relaxation of Mn^{II} (**Fig. S6c**).

Cyclic Voltammetry

The electrochemical behaviour of the porphyrin TPFPP(PEG)$_4$ (**2**) and the metalloporphyrins Mn^{III}-TPFPP(PEG)$_4$ (Mn^{III}-**3**) and Zn^{II}-TPFPP(PEG)$_4$ (Zn^{II}-**3**) was investigated in deoxygenated 0.1 M HEPES buffer solution, pH 7.4, by cyclic voltammetry at a glassy carbon electrode (GCE). The cyclic voltammograms obtained for the fluorinated porphyrins are presented in **Fig. 2a**. No adsorption of any porphyrin was observed in consecutive cycles.
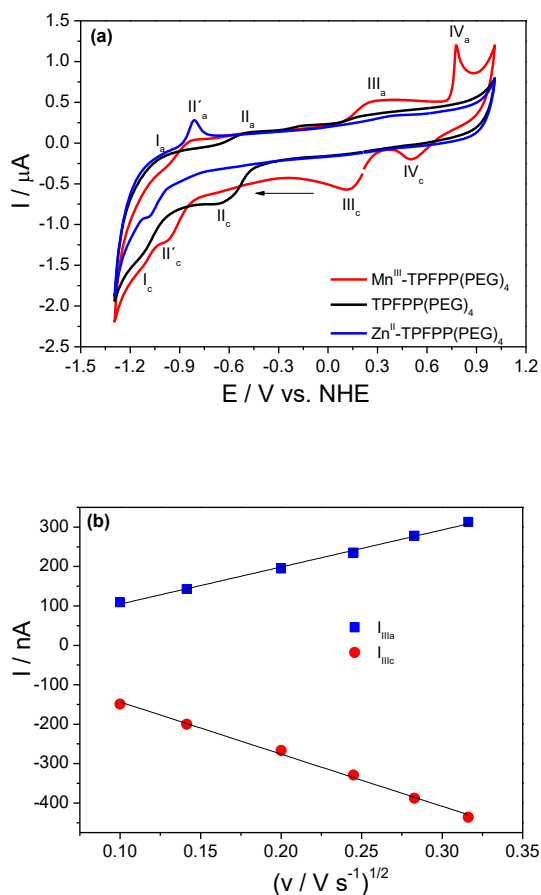

Figure 2. a) Cyclic voltammograms at GCE in 0.1 M HEPES buffer pH 7.4 for 2.2 mM of TPFPP(PEG)$_4$ (black), Mn^{III}-**3** (red) and Zn^{II}-**3** (blue); b) Plot of the peak current versus square root of scan rate for the peaks III$_a$/III$_c$, corresponding to Mn^{II}/Mn^{III} for the CV of 2.2 mM Mn^{III}-**3** in 0.1 M HEPES buffer pH 7.4 at scan rates 10-100 mV s^{-1}

In the potential range investigated, which is limited by water reduction and oxidation potentials, the following behavior was observed. The free porphyrin exhibited two redox couples II$_a$/II$_c$ and I$_a$/I$_c$, with midpoint potential $E_{pII}{}^m$= -0.580 V and peak separation ΔE_{pII} = 0.120 V and $E_{pI}{}^m$= -1.060 V and peak separation ΔE_{pI} = 0.120 V, respectively. These couples were ascribed to the porphyrin ring two successive one-electron oxidation/reduction processes, the first involving a π-radical anion and the second the porphyrin dianion formation, respectively, as suggested in the litterature.[66,67] The formal potential for these peaks shifted to more negative values for Mn^{III}-**3** ($E_{pII'}{}^m$= -0.900 V), as well as for Zn^{II}-**3** ($E_{pII'}{}^m$= -0.945 V) porphyrins, which is expected with the introduction of a metal ion in the porphyrin by its effect on the electronic structure of the macrocyclic ring. For Zn^{II}-**3** no additional peaks were observed in the

potential range studied; those involving oxidation of the porphyrin ring should be higher than +1.20 V (see later). In the case of Mn^{III}-**3** two more redox couples III$_a$/III$_c$ and IV$_a$/IV$_c$ appeared. The III$_a$/III$_c$ pair with $E_{pIII}{}^m$ = +0.193 V and ΔE_{pIII} = 0.150 V was assigned to the Mn^{II}/Mn^{III} redox process, while IV$_a$/IV$_c$ with $E_{pIV}{}^m$= +0.642 V and ΔE_{pIV} = 0.264 V was associated with the Mn^{III}/Mn^{IV} reaction. These assignments were confirmed by performing cyclic voltammetry under the same conditions in the presence of Mn^{III}-acetate (**Fig. S7a**), where two redox couples also appeared. The pair IV$_a$/IV$_c$ exhibited potential values $E_{pIV'}{}^m$= +0.575 V and $\Delta E_{pIV'}$ = 0.222 V for Mn^{III}-acetate, quite similar to those of Mn^{III}-**3** and of the cationic tetramethyl meso-substituted porphyrin, Mn^{III}-PMPyP, at basic pH.[68-70] The reversibility of this redox process was found not to depend on experimental conditions[71] and will not be further discussed here. However, for the pair III$_a$/III$_c$ a large difference was observed; the peak separation was wider $\Delta E_{pIII'}$ = +0.778 V, whilst the formal potential was more negative, $E_{pIII'}{}^m$= -0.065 V for Mn^{III}-acetate. An increase in peak current was also observed for the same redox couple, III$_a$/III$_c$, a factor of 2 for the oxidation and 3 for reduction process in the case of the Mn^{III}-**3** porphyrin compared with Mn^{III}-acetate. Thus, the introduction of manganese into the porphyrin has a positive impact, by greatly increasing its reversibility with regard to the Mn^{II}/Mn^{III} process. An improvement in the Mn^{II}/Mn^{III} redox reaction was also achieved when introducing manganese in a sulphonated porphyrin, Mn^{III}-TPPS$_4$, since this redox pair exhibited a peak separation $\Delta E_{pIII''}$ = 0.252 V with midpoint potential $E_{pIII''}{}^m$= -0.238 V (data not shown). However, the formal potential for Mn^{III}-**3** is more positive and the peaks are less separated, as well as exhibiting higher current peaks, compared with Mn^{III}-TPPS$_4$, which enables the former porphyrin to be elected as a better redox probe. Although the Mn^{II}/Mn^{III} redox reaction in Mn^{III}-**3** was a quasi-reversible slow electron transfer, this is in agreement with what was found for non-fluorinated Mn-porphyrins, eg. Mn^{III}-TPPS$_4$, with $E_{pIII}{}^m$ values of -0.24 V in DMF/0.1 M TBAP[72] and -0.22 V in water/0.3 M Na$_2$SO$_4$.[73], as well as for manganese fluorinated porphyrin, Mn-TPFPP, in acetonitrile[61], $E_{pIII}{}^m$ value of +0.05 V **(Table S1)**.

The cyclic voltammetric behaviour of the Mn^{III}-**3** porphyrin was investigated over a range of scan rates from 10 to 100 mV s^{-1}. The results showed a linear dependence of the anodic and cathodic peak currents of the redox couple Mn^{II}/Mn^{III} with the square root of the scan rate (v) (**Fig. 2b and S7b**), indicating a diffusion-controlled electron transfer process,[74] in agreement with what was previously observed for the complex Mn^{III}-HBET (HBET = N-(2-hydroxybenzyl)-N,N´N´-ethylenediaminetriacetic acid)[26] and other manganese-based porphyrins.[75] The stability of the Mn^{III}-**3** porphyrin was checked by performing cyclic voltammograms of the prepared solution over a period of one month. No change in peak current values was observed, indicating high stability of this compound in aqueous solution. In spite of the quasi-reversible process, the value of the redox potential achieved as well as its high stability ensures the ability of Mn^{III}-**3** to act as a redox probe, as proposed here.

The redox behaviour of the free porphyrin and the Zn^{II}-**3** and Mn^{III}-**3** derivatives was also investigated by cyclic voltammetry in DCE and 0.6 M Bu$_4$NBF$_4$ at a glassy carbon electrode **(Table S1** and **Fig. S7d,e)**. The free porphyrin showed two redox couples at negative potentials with $E_p{}^m$ values at -0.452 V and -1.00 V, corresponding to the porphyrin ring anion and dianion formation. Zn^{II}-**3** showed two

reversible monoelectronic reduction peaks with E_p^m values at -0.72 V and -1.10 V, also assigned to the reduction of the porphyrin ring to the π-radical anion and dianion forms. The reversible monoelectronic reduction peak observed at -1.31 V and the irreversible peak at -1.64 V correspond to the PEG chains. Zn^{II}-**3** also exibited two irreversible monoelectronic anodic peaks at +1.61 V and +1.80 V, corresponding to the oxidation of the pyrrole groups to the radical cation and dication forms of the Zn porphyrin. This was followed by a multielectronic irreversible wave at + 2.80 V, corresponding to the degradation of the ether chains in the porphyrin. These data are in agreement with reported data for other perfluorinated Zn^{II} porphyrins (**Table S1**).[65, 66, 76] The Mn^{III}-**3** porphyrin exhibited a similar behaviour to that observed in aqueous media: at negative potentials two redox couples with E_p^m values at -0.828 V and -1.131 V, corresponding to porphyrin ring anion and dianion formation. These assignments were confirmed by comparison with the data obtained for the free porphyrin, which show a trend in the potentials involving the reduction of the porphyrin moiety to be less negative for the free porphyrin than in the Zn^{II}-**3** and Mn^{III}-**3** complexes, as also observed in HEPES buffer. The Mn^{II}/Mn^{III} core redox process in the Mn^{III}-**3** porphyrin was observed at E_p^m = +0.335 V, with a peak separation ΔE_p = 0.350 V, again in agreement with data for other perfluorinated Mn^{III} porphyrins (**Table S1**).[65, 66, 76] All the redox potentials obtained simultaneously in the two solvents were found to be lower in H_2O

than in DCE, in agreement with their relative dielectric constants and complexing abilities.

Conversion between the Mn^{III}-3 and Mn^{II}-3 redox states

In order to evaluate the possibility of reduction of Mn^{III}-**3** to Mn^{II}-**3**, two different biological reductants were used, ascorbic acid and BME. The reduction with ascorbic acid was followed by UV-Vis spectra, recorded in PBS (phosphate buffer solution) in a solution of the Mn^{III}-**3** porphyrin upon addition of increasing amounts of reductant (**Fig. 3a**). Addition of 0.28 equivalents of ascorbic acid caused a decrease in the absorption at 457 nm (typical wavelength for the charge transfer Soret band (band V) of Mn^{III} porphyrins), with the concomitant appearance of a new band at 434 nm, which is a typical absorption wavelength for Mn^{II} porphyrins.[77] Total reduction of Mn^{III}-**3** to Mn^{II}-**3** was achieved after the addition of 25.3 equivalents of ascorbic acid. Conversely, oxidation of Mn^{II}-**3** to Mn^{III}-**3** was evaluated by acquiring the UV-Vis spectra of a Mn^{II}-**3** PBS solution, following exposure to air for 10 min, 4 h and 24 h (**Fig. 3b**). The system displays complete reversibility after 24h. A similar study was performed with BME and complete reduction from Mn^{III}-**3** to Mn^{II}-**3** was achieved in the presence of 48 equivalents of this reductant (**Fig. 3c**). In this case, total reoxidation by air exposure was achieved after 72h (**Fig. 3d**).

Figure 3 a) UV-Vis reduction titration of 0.041mM Mn^{III}-**3** with ascorbic acid, recorded in PBS (25 ºC, pH = 7.4). Number of equivalents of ascorbic acid added: (black line) - 0; (red line) – 0.28; (light blue line) – 0.57; (light green line) – 0.85; (pink line) – 6.4; (dark green) – 11.4; (dark blue) – 25.3; **b)** UV-Vis spectra of the reoxidation of Mn^{II}-**3** upon air exposure: (black line) – Mn^{III}-**3** before exposure; (red line) – after 10 min. exposure; (blue line) after 4h exposure; (green line) complete conversion to Mn^{III}-**3** (after 24h expos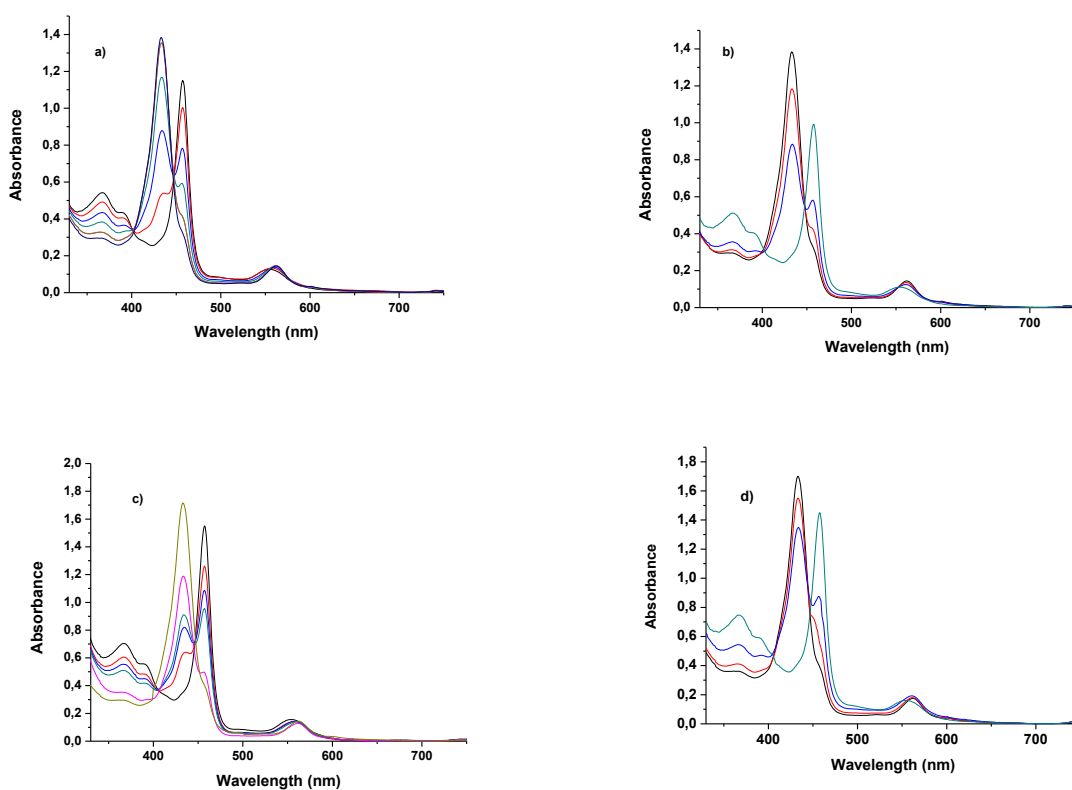ure). **c)** UV-Vis reduction titration of 0.041mM Mn^{III}-**3** with BME, recorded in PBS (25 ºC, pH = 7.4). Number of equivalents of BME added: (black line) - 0; (red line) – 0.43; (light blue line) – 2.32; (light green line) – 7.94; (pink line) – 23.5; (dark green) – 48; **d)** UV-Vis spectra of the reoxidation of Mn^{II}-**3** upon air

exposure: (black line) – Mn^{II}-**3** before exposure; (red line) – after 30 min. exposure; (blue line) after 24 h exposure; (green line) complete conversion to Mn^{III}-**3** (after 72 h exposure).

In contrast, reoxidation of Mn^{II}-**3** by addition of an increasing number of equivalents of hydrogen peroxide showed no reversibility to Mn^{III}-**3** (**Fig. S8**). Although the addition of up to the first equivalent gave mostly Mn^{III}-**3**, further addition of a large excess led to formation of Mn^{IV} and Mn^{V} oxo derivatives (Soret bands in the 424-443 nm region),[69, 70] in agreement with the literature.[77,78]

Besides the quite different wavelengths of the Soret band, the UV-Vis spectra of Mn^{III}-**3** and Mn^{II}-**3** show other distinctive differences **(Fig. S9)**. In the UV region, Mn^{III}-**3** shows two other bands, (VI and Va), less intense than the Soret band, at 367 and 391 nm, respectively, which in Mn^{II}-**3** dramatically decreases intensity and shifts to 364 nm (VI), or disappears (Va). In the visible region, Mn^{III}-**3** displays a QIV band at 554 nm, which is shifted to 561 nm upon reduction, but the QIII band, usually observed in the 610-620 nm range, is not visible.[64, 72, 77] The absence of a decreased intensity of the Soret band and the absence of a band above 700 nm, show that the porphyrin macrocycle is not reduced.[79]

In order to determine the empirical rate law for the reduction of Mn^{III}-**3** by ascorbic acid, a series of kinetic experiments were conducted at 25°C (pH=7.4) under pseudo-first order conditions, following the disappearance of the Soret band at 457 nm (ε = 1.01×10^4 M^{-1}s^{-1}) over time in 50 ms intervals. Initial reaction rates were measured first at three different ascorbic acid concentrations (91, 191 and 390 μM) keeping the initial Mn^{III}-**3** concentration constant at 8 μM, and then at three different initial Mn^{III}-**3** concentrations (95, 150 and 330 μM) in the presence of 9.8 mM ascorbic acid. The experimental data (**Figs. S10** and **S11**) evidenced that the reduction is first-order in relation to both Mn^{III}-**3** and ascorbic acid concentrations, with an overall second-order rate constant k_2 = 46.1 ± 5.6 M^{-1} s^{-1}. Similar experiments with BME as reductant yielded a k_2 value of 13.8 ± 1.1 M^{-1} s^{-1}. These values are one to two orders of magnitude larger than the corresponding value of k_2 = 0.38 M^{-1} s^{-1} reported for the reduction of Mn^{III}-HBET by glutathione.[26] The normal blood plasma concentration of ascorbic acid is in the 20-40 μM range, which can be somewhat reduced in some pathologies, such as systemic inflammation.[80, 81] For this ascorbic acid concentration range, the half-life of Mn^{III}-**3** is roughly 6-13 min. Ascorbic acid accumulates in circulating immune cells, such as neutrophiles, monocytes and lymphocytes, reaching up to 1.2 to 3.5 mM concentrations.[81] In this range of concentrations, the half-life of Mn^{III}-**3** would be expected to decrease to about 4 -12 s if it could enter those cells. Ascorbic acid, present in neutral solution predominantly in the monoanionic form (HA$^-$), can be oxidized to dehydroascorbic acid, which appears in solution in the hydrate form Hy, with $E^{o\prime}_{Hy/HA^-}$ = +0.184 V in 0.1 M HEPES buffer pH 7.4 (**Fig. S7c**), which is slightly lower than the value + 0.276 V reported in phosphate buffer.[82] This value is low enough to reduce the metal center of Mn^{III}-**3** ($E^{o\prime}_{Mn(III)/Mn(II)}$ = +0.193 V) (K_{eq} $\cong$ 1 at 298 K) when present in excess, as in our experimental conditions. BME is a non-natural thiol ($E^{o\prime}$ = -0.26 V)[83] also capable of reducing Mn^{III}-**3**. A similar study with an aqueous solution of Mn^{III}-TPPS$_4$ showed that no reduction was observed in the presence of ascorbic acid, which is in agreement with the reported redox potential of Mn^{III}-TPPS$_4$ in aqueous solution ($E^{o\prime}_{Mn(III)/Mn(II)}$ = -0.22 V).[73]

Reduction of Mn^{III}-**3** to Mn^{II}-**3** was not observed in the presence of glutathione even in a large excess of this important biological reductant. This is thermodynamically unexpected on the basis of their redox potentials, as the $E^{o\prime}$ value (-0.240 V)[10] of the GSSG/2GSH couple is negative enough to reduce Mn^{III}-**3**, as observed with BME. In order to rationalize this finding, we have compared the ^{13}C NMR spectrum of glutathione in the absence and in the presence of 0.1 equivalent of Mn^{III}-**3** in D$_2$O **(Fig. S12)**. The addition of Mn^{III}-**3** causes broadening of specific glutathione ^{13}C resonances: the two carboxylate peaks at 173.52 and 172.30 ppm ($^-$O-**C**=O) and the signals of neighbouring carbons at 53.58 ppm ($^-$COO-**C**-NH$_2$) and 41.46 ($^-$COO-**C**-NH-). This can be attributed to the binding of the terminal carboxylate groups of glutathione to the paramagnetic metal ion in the axial position of Mn^{III}-**3**. Such binding mode is in agreement with X-ray crystal structures reported for complexes of Mn^{III}-porphyrins with trichloroacetate.[64] On the other hand, we have shown above that electron transfer occurs with BME which has no carboxylate group. Altogether, this suggests that the coordination of glutathione to Mn^{III}-**3** to form a ternary complex blocks the electron transfer between the thiol group and the metal center and prevents the reduction. For the same reasons, reduction of Mn^{III}-**3** to Mn^{II}-**3** was also not observed, even in the presence of a large excess of cysteine (data not shown).

Relaxivity studies

The relaxation properties have been investigated for both the oxidized Mn^{III} and the reduced Mn^{II} form of the porphyrin complex **3**. Mn^{II}-**3** was obtained by adding 30 equivalents of ascorbic acid to the Mn^{III} analogue. Full conversion of Mn^{III}-**3** to Mn^{II}-**3** was evidenced by recording UV-Vis spectra before the relaxivity measurements. The NMRD profiles recorded at 25 °C for the reduced and for the oxidized form are presented in **Fig. 3.**

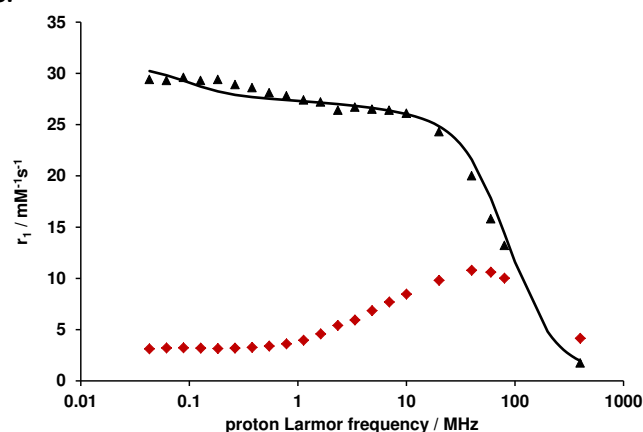**Figure 4.** Proton NMRD profiles recorded at 298 K for Mn^{III}-**3** (red ♦) and Mn^{II}-**2** (black ▲). The curve represents the least squares fit to the data points as explained in the text.

The reduction of the d^4 Mn^{III}-**3** complex to the electronically more symmetric d^5 Mn^{II}-**3** analogue leads to a large increase in

the proton relaxivities at low and medium magnetic fields. Although a similar trend has been previously found for the Mn^{II}/Mn^{III}-TPPS$_4$ and Mn^{II}/Mn^{III}-TPPBr$_6$S$_4$ analogues,[59, 84] it was observable only in a much more restricted frequency range. Indeed, for those TPPS$_4$ analogues, the two curves cross each other at ~10 MHz,[59] while for our system, even at 80 MHz, the relaxivity of the reduced form remains ~30% higher than that of the oxidized form. On MR images, this would correspond to a remarkable "turn-on" response to a reducing environment.

As shown by Koenig[34] and later by Bryant,[84] attempts to fit the NMRD data for the oxidized Mn^{III}-TPPS$_4$ by using the Solomon-Bloembergen-Morgan theory do not yield satisfactory results for many of the fitted parameters. These include the distance between the Mn^{III} ion and the protons of the coordinated water molecules, r_{MnH}, that showed highly temperature-dependent values ranging from 2.13 Å (35 ºC) to 2.48 Å (5 ºC), which is way too short in the light of the structural data available from X-ray crystallographic studies.[85] They also used a value for the water exchange rate, $k_{ex}^{298} = 10^9$ s^{-1} which is too large when compared with k_{ex}^{298} values of 14×10^6 s^{-1} and 27.4×10^6 s^{-1} determined from the temperature dependence of ^{17}O NMR relaxation times.[86, 87] It was indeed evidenced that the relaxation mechanism of Mn^{III} porphyrin derivatives has unique aspects, the most important being the unusual role of ZFS interactions and the effect of these interactions on the electron spin dynamics.[35] Consequently, the analysis of the NMRD curves of Mn^{III}-**3** requires a complex mathematical treatment which, in the case of Mn^{III}-TPPS$_4$ gave a reasonable and temperature-independent r_{MnH} value of 2.80 Å. Values for other parameters were also calculated. At 20 ºC a value of the rotational correlation time, $\tau_R = 900$ ps and two different electron spin relaxation times $\tau_S^{(\pm1)} = 506$ ps and $\tau_S^{(\pm2)} = 180$ ps for the $M_S = \pm1$ and ±2 non-Kramers manifolds, respectively, were reported.[35] When compared with the corresponding calculated SBM parameters,[84] $\tau_R = 275$ ps and the parameters describing the electron spin relaxation, the correlation time for the modulation of the zero-field-splitting, $\tau_v = 30$ ps and the electron spin relaxation time at zero magnetic field, $\tau_{SO} = 15$ ps, one concludes that the SBM treatment underestimated τ_R and τ_{SO} and gave a too long τ_v value. However, such a mathematical treatment for the analysis of the NMRD curves of Mn^{III}-**3** is beyond the scope of the present work. Despite this, our observation that the r_1 values of Mn(III)-**3** at low fields are systematically lower than those of Mn^{III}-TPPS$_4$ [59, 84] can be qualitatively explained by their relative electronic relaxation parameters, which dominate r_1 at such fields. Thus, we can say that Mn(III)-**3** has faster electronic relaxation than Mn^{III}-TPPS$_4$ as a result of the fluorinated phenyl substituents at the porphyrin meso positions.

Concerning the Mn^{II}-**3** complex, its NMRD curve has been analysed within the frame of the SBM theory (see ESI for equations). The outer sphere relaxation contribution was considered according to the translational diffusion model developed by Freed.[88] There are a large number of parameters that enter in the analysis and some of them have been fixed to reasonable values. These involve the distance between the Mn^{II} electron spin and the proton of the coordinated water

molecules ($r_{MnH} = 3.1$ Å), the distance of closest approach of water protons diffusing around the complex which determines the outer sphere interactions ($a_{MnH} = 3.6$ Å) and the relative translational diffusion coefficient ($D_{MnH} = 26 \times 10^{-10}$ m^{2}s^{-1}). The hydration number was also fixed to $q = 2$, in analogy to the TPPS$_4$ analogue. In the fit, we adjusted the rotational correlation time, τ_R, the parameters describing electron spin relaxation, τ_v, the correlation time for the modulation of the zero-field-splitting and Δ^2, the energy of the zero-field-splitting. The water exchange rate could not be measured for Mn^{II}-**3** by variable temperature ^{17}O NMR, as it is typically done for paramagnetic complexes, due to solubility problems at higher temperatures. Therefore, we also adjusted this parameter. The fit is rather satisfactory (**Fig. 3**) and the resulting parameters are given in **Table 1**, in comparison to some other Mn^{II} complexes. We should note that the inclusion of a scalar relaxation mechanism into the fit by assuming a scalar coupling constant of $A_h = 0.5$ MHz did not improve the quality of the fit and did not have an important effect on the other fitted parameters.

Table 1. Relaxivities and fitted parameters for Mn^{II}-**3** and other Mn^{II} complexes from literature.

Parameter	Mn^{II}-**3**	[Mn(**15-py N$_3$O$_2$**)(H$_2$O)$_2$]$^{2+}$ [89]	[Mn(H$_2$O)$_6$]$^{2+}$ [90]
r_1 / mM^{-1} s^{-1} 20 MHz/298 K	24.3	4.48	7.4[a]
k_{ex}^{298} / 10^6 s^{-1}	0.81±0.2	3.8	21
τ_{rH}^{298} / ps	4800±1000	40.3	30[b]
τ_v^{298} / ps	5±1	3.3	3.3
Δ^2 / 10^{18} s^{-2}	0.50±0.2	6.6	5.6

[a]this work; [b]308 K.[91]

Bryant *et al.* reported some time ago on the analysis of the NMRD profile of Mn^{II}TPPS$_4$.[84] They concluded that it was impossible to describe the Mn^{II}TPPS$_4$ system by the SBM theory and with a reasonable set of parameters. In their best fit, they used a reasonable $k_{ex}^{298} = 10^7$ s^{-1}, $\tau_R^{298} = 300$ ps and a very short $\tau_v^{298} = 0.5$ ps. The outer sphere contribution was parametrized with a very short distance for the closest approach of water protons to the manganese center ($a_{MnH} = 2.0$ Å) and a very small value for the diffusion constant (6×10^{-10} m^{2}s^{-1}). To explain these discrepancies, they proposed that the dipole-dipole approximation of the SBM theory might fail for these porphyrin complexes which can undergo an electron spin delocalization from the manganese ion to the porphyrin. This hypothesis seemed to be supported by the fact that a derivative, Mn^{II}-TPPBr$_6$S$_4$, which was brominated on the pyrrole rings, had even higher proton relaxivities. In our analysis, the Mn^{II}-proton distances and the diffusion constant have values typical of Mn^{II} chelates. The water exchange rate is also reasonable. The rotational correlation time has a high value, but it is not surprising given the presence of four PEG chains attached to the porphyrin ring. The fact that the paramagnetic metal is in the barycenter of a large molecule implies that it takes full benefit from the slow rotation of the whole molecule. A porphyrin center bearing four Gd^{III} complexes, with a similar molecular weight ($M_w = 2.76$ kDa), thus molecular size, as that of Mn^{II}-**3** ($M_w = 2.99$ kDa) has been recently reported.[92] Here the

paramagnetic Gd^{III} complexes are not in the barycenter of the molecule. However, the relaxivities have been analyzed with the Lipari-Szabo approach that allows calculating the global rotational correlation time, τ_g, which can then be related to the rotational motion of the entire molecule. The global rotational correlation time for this tetra-Gd porphyrin was found to be τ_g = 2.3 ns, similarly in the nanosecond range as the τ_R calculated for Mn^{II}-**3**. This gives confidence in the fit of the NMRD profile for Mn^{II}-**3**. Even if the errors on the calculated parameters might be higher than usual given the lack of independent determination for the water exchange rate, their order of magnitude should be correct.

Evaluation of the cytotoxicity of Mn^{III}-3 in a cell model

The *in vitro* cytotoxicity of Mn^{III}-**3** on the epithelial HeLa tumor cell line was evaluated using the Alamar Blue colorimetric assay. The cells were incubated with solutions containing different concentrations of Mn^{III}-**3** (0.25–5mM), prepared from a PBS stock solution and diluted in DMEM complete medium, during different time periods (2 h, 4 h and 24 h). The Mn^{III}-**3** compound was soluble in aqueous solution and the tested concentrations were in the meaningful range for the desired biomedical application.

As shown in **Fig. 4**, no statistically significant toxicity was observed after 2 and 4 h of incubation for all the concentrations used. After 24 h exposure to the compound, a statistically significant decrease in cell viability was observed for the highest concentrations tested (3 and 5 mM). In addition to its water solubility, the absence of statistically significant citotoxicity of Mn^{III}-**3** in the concentration and exposure time ranges normally used in *in vivo* MRI, are positive indications for its potential application as a redox-responsive agent.
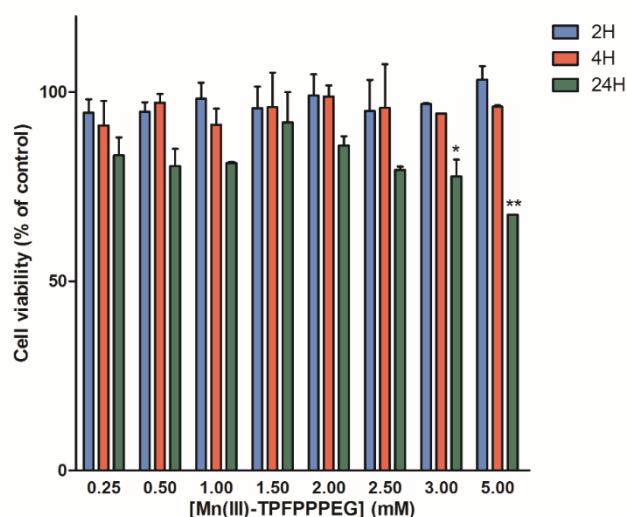

Figure 5. Effect of increasing concentrations the Mn^{III}-**3** porphyrin compound on HeLa cells viability as a function of time. HeLa cells were plated in 96-well plates at a density of $2x10^4$ cells per well. Twenty-four hours after plating, the cells were incubated with 0.25, 0.5, 1.0, 1.5, 2.0, 2.5, 3.0 and 5.0 mM solutions of Mn^{III}-**3**. Cell viability was measured after 2, 4 or 24 h using the Alamar blue assay. Cell viability is presented relative to the percentage of untreated cells (control cells) considered as 100%. Data represent the mean ± SD of three independent experiments. Pairwise data comparisons were performed between cell viability values obtained with each Mn^{III}-**3** concentration, as compared with the immediately precedent concentration, for each incubation period (non-significant) and between cell viability values obtained for each incubation period with Mn^{III}-**3**, as compared with the immediately precedent incubation period, for each concentration (**p<0.01, *p<0.05). The significance of the results was statistically analyzed by one-way analysis of variance (ANOVA) with Tukey's multiple pairwise comparison. Statistical significance was set at p < 0.05.

Conclusions

A new water-soluble fluorinated porphyrin derivative conjugated with PEG chains was synthesized. It is capable of stabilizing both Mn^{III} and Mn^{II} oxidation states in a biologically relevant range of redox potentials. In aqueous solution, Mn$^{III/II}$-**3** undergoes reversible reduction/oxidation reactions, promoted by the natural reducing agent ascorbic acid and oxygen, respectively. The reduction process with ascorbic acid has second-order kinetics, with a k_2 value of 46.1 M^{-1}s^{-1}, which is two orders of magnitude larger than the k_2 of 0.38 M^{-1} s^{-1} reported for the reduction of Mn^{III}-HBET by glutathione.[26] Re-oxidation is slowly but fully achieved by air oxygen.

Interestingly, ^{19}F NMR resonances of Mn^{III}-**3** are relatively sharp which could open further possibilities to exploit such complexes as paramagnetic ^{19}F NMR probes.[93]

At medium frequencies (20-80 MHz), the relaxivity increase between the Mn^{III}-**3** and Mn^{II}-**3** complexes is considerably improved with respect to the previously studied Mn-TPPS$_4$ analogue[59] (at 40 MHz, Δr_1 ~100 %). Cytotoxicity evaluation on epithelial HeLa cells confirmed *in vitro* non-toxicity of the compound in the mM concentration range typically used for MR imaging.

In general, the development of MRI imaging probes to monitor redox environments *in vivo* faces several difficulties. Mn$^{II/III}$ chelates of open-chain hydroxybenzyl-ethylenediamine acetic acid derivatives have been reported to possess favorable *in vitro* properties as redox active MRI contrast agents,[30] but their kinetic stability might be insufficient. In this respect, Mn-porphyrin redox responsive probes can be advantageous.

The present Mn^{II}/Mn^{III}-porphyrin couple satisfies many of the criteria required for a redox imaging probe: good water solubility, biocompatibility, non-toxicity, thermodynamic and kinetic stability in both metal oxidation states, a redox half-cell potential accessible to biologically relevant reducing agents with fast kinetics (adapted to the imaging time scale), and a strong "turn on" relaxivity response upon reduction. However, it is not reduced by glutathione or cysteine, the major thiol-disulfide redox buffers of the intracellular and extracellular spaces, respectively. In human plasma, cysteine-cystine and glutathione reach levels of ~260 microM and ~7 microM, respectively,[94] while ascorbic acid has 20-40 microM concentration.[80, 81] Therefore, the role of ascorbic acid should not be ignored either in maintaining the extracellular redox state. Our redox sensitive MRI probe might have potential to report, with fast kinetics (few minutes half-life), on extracellular ascorbate without the interference of the cysteine-cystine buffer. In circulating immune cells for instance, ascorbic acid amounts to millimolar concentrations and controls the redox state. Provided the probe is modified for cell internalization to reach mM concentrations, it could be useful to assess intracellular ascorbic acid in such cells with very fast kinetics (few seconds half-life).

Furthermore, MRI quantification of ascorbate could be also achieved by separating the effect of the *in vivo* concentration of the probe from the redox effect on the observed contrast. For this, a

ratiometric technique could be used,[95] based on injecting a cocktail of the [52]Mn-radiolabeled porphyrin and the normal one. Indeed, [52]Mn ($t_{1/2}$ = 5.59 d, β^+ = 29.6%, $E_{\beta ave}$ = 0.24 MeV) is a promising positron emission tomography (PET) radioisotope,[96] which allows to directly combine PET and MRI detection. The advantage of this technique is the identical biodistribution of the PET and MRI probes. As PET is a quantitative technique, it will allow assessing the concentration of the MRI probe as well, leading to quantification of the ascorbate concentration.

Experimental Section

Materials and methods

Commercially available reagents were bought from Aldrich, except PEG500 (mono methyl polyethyleneglycol) (Fluorochem) and used as received. All solvents were pre-dried according to standard laboratory techniques. For the cyclic voltammetry experiments, 1,2-dichloroethane (DCE) was purchased with the highest quality available, and stored in molecular sieves, under inert atmosphere. The other reagents were also purchased with the highest quality available and were used as received. 5,10,15,20-(pentafluorophenyl)porphyrin was synthesized according to the literature.[64] UV-visible absorption spectra were recorded on a Hitachi U-2010 using quartz cells. The molar absorption coefficients were determined using PBS as solvent. ^{1}H-NMR and ^{19}F-NMR spectra were recorded on a 400 MHz Bruker Avance III NMR spectrometer (400.101 and 376.5MHz respectively). Proton chemical shifts are given in parts per million (ppm) relative to tetramethylsilane at δ 0.00 ppm and ^{19}F relative to TFA at δ -76.55 ppm. Mass spectra (ESI-FIA-TOF) were acquired using an Applied Biosystems Voyager DE-STR instrument equipped with a nitrogen laser (λ = 337 nm).

Synthesis

5,10,15,20-(4-PEG500-2,3,5,6-fluorophenyl)porphyrin (TPFPP(PEG)₄, 2)

A mixture of 5,10,15,20-(pentafluorophenyl)porphyrin (140 mg, 0.14 mmol) and PEG500 (mono methyl polyethyleneglycol - Mw = ~500 Da) (0.359 mL, 0.718 mmol) was dissolved in 10 mL of dry DMF. After the addition of NaH (17 mg, 0.718 mmol) the reaction was left at room temperature, until complete consumption of 5,10,15,20-(pentafluorophenyl)porphyrin, checked by TLC (2 hours). The reaction mixture was extracted several times with dichloromethane/water and dichloromethane/aqueous 1M K_2CO_3 and the organic layer was dried over anhydrous sodium sulfate and concentrated under vacuum. Porphyrin **2** was obtained in 78% yield. ^{1}H NMR (400 MHz, CDCl₃) δ, ppm: 8.93 (s, 8 H_β), 3.65-3.60 (m, 160 - 196 (polydisperse distribution) H_{PEG}), -2.90 (s, 2 H_{NH}); ^{19}F NMR (376 MHz, CDCl₃) δ, ppm: -138.86-(-138.04) (m, 4F), -157.97-(-157.03) (m, 4F). MS (ESI-FIA-TOF) m/z: 1028.3720, 1220.9980, 1287.0377, 1491.1818 $[M]^{2+}$ (polydisperse distribution).

Mn^III-5,10,15,20-(4-PEG500-2,3,5,6-fluorophenyl)porphyrin (Mn^III-TPFPP(PEG)₄ , Mn^III-3)

Free base **2** (100 mg, 0.045 mmol), sodium acetate (367 mg, 4.47 mmol) and manganese (II) acetate were dissolved in 3 mL of acetic acid. The reaction was stirred at 80 ºC and controlled by UV-Vis spectroscopy. After complete conversion to the manganese complex (2 hours), the reaction mixture was extracted several times with dichloromethane/water and then the organic layer was dried over anhydrous sodium sulfate and concentrated under vacuum. Porphyrin **3** was obtained in 85% yield. MS (ESI-FIA-TOF) m/z: 1121.3612, 1319.9802, 1386.0195, 1493.6057 $[M]^{2+}$ (polydisperse distribution).

Zn^II-5,10,15,20-(4-PEG500-2,3,5,6-fluorophenyl)porphyrin (Zn^II -TPFPP(PEG)₄, Zn^II-3)

Free base 2 were dissolved in a mixture of chloroform/methanol (2:1) and zinc(II) acetate was added. The reaction was stirred at 50ºC and controlled by UV-Vis spectroscopy. After complete conversion (1h) the reaction mixtures was extracted several times with dichloromethane/water and the organic phase was dried over anhydrous sodium sulfate and concentrated under vacuum. The zinc derivative was obtained in 89% yield. ^{1}H NMR (400 MHz, CDCl₃) δ, ppm: 8.88 (s, 8 H_β), 3.67-3.12 (m, 160 - 196 (polydisperse distribution) H_{PEG}). MS (ESI-FIA-TOF) m/z: 1445.0650, 1467.0780, 1489.0912, 1511.1044 $[M]^{2+}$ (polydisperse distribution).

Mn^III-5,10,15,20-tetrakis(4-sulfonatophenyl)porphyrin (Mn^IIITPPS₄)

TPPS₄ was synthesized according to literature.[97] Mn^IIITPPS₄ was obtained using the same procedure used for the porphyrin Mn^III-3. Characterization is in accordance to literature. [67]

Electron Paramagnetic Resonance (EPR)

X-band (0.34 T, 9.5 GHz) continuous wave (CW) EPR measurements were carried out on a Bruker EMX spectrometer, equipped with a continuous flow Oxford Instruments cryostat for low temperature measurements. The EPR experiments were performed on the Mn^II salt MnCl₂ and Mn^III-porphyrin samples in aqueous solution at 25 ºC. (see supporting information). Simulation of the experimental spectra of aqueous Mn^{2+} was performed using SimFonia v.1.2 (Bruker Instruments Inc. software). The EPR spectra showed that the residual Mn^{2+} aqueous ion concentrations present in the Mn^III-porphyrin solutions used for the NMRD measurements were lower than 10 μM.

[1]H Relaxometry

The longitudinal (T_1) proton relaxation times of aqueous solutions of the Mn^III and Mn^II complexes were measured at 25 ºC and 37 ºC by nuclear magnetic resonance relaxometry on a Bruker Minispec mq20 relaxometer operating at a magnetic field of 0.47 T, corresponding to a proton Larmor frequency of 20 MHz, using an inversion recovery pulse sequence. All the experimental values were corrected taking into account the diamagnetic contribution of water. The corresponding relaxivity values (r_1), were calculated through the least-squares curve fitting of the inverse relaxation time $1/T_1$ (s^{-1}) vs. the Mn^II/III

concentration. ^{1}H NMRD (Nuclear Magnetic Relaxation Dispersion) profiles were recorded on a Stelar SMARtracer Fast Field Cycling NMR relaxometer (0.01-10 MHz) and a Bruker WP80 NMR electromagnet (20, 40, 60 and 80 MHz) adapted to variable field measurements and controlled by a SMARtracer PC-NMR console. The temperature was monitored by a VTC91 temperature control unit and maintained by a gas flow. The temperature was determined by previous calibration with a Pt resistance temperature probe. The longitudinal relaxation rates ($1/T_1$) were determined in water at 25 ºC and 37 ºC. High field relaxivities were measured on a Bruker AVANCE NMR spectrometer at 400 MHz by placing the sample solution in an inner co-axial tube while the outer tube was filled with D_2O.

Reduction kinetics

To stock 1.35×10^{-5} M solutions of Mn^{III}-**3** in PBS (25ºC, pH = 7.4) were added appropriate volumes of 50 mM ascorbic acid or of 63 mM BME. For one set of experiments, the final concentration of Mn^{III}-**3** was kept at 0.008 mM and ascorbic acid was 0.390 mM, 0.191 mM and 0.091 mM. For the other set, the final concentration of ascorbic acid was constant at 9.7 mM and Mn^{III}-**3** was 0.230 mM, 0.150 mM and 0.095 mM. The same final concentrations were used for the BME experiments.

The conversion of Mn^{III}-**3** to Mn^{II}-**3** was monitored by the disappearance of a strong UV-Vis absorbance at 457 nm ($\varepsilon = 1.01 \times 10^4$ M^{-1}s^{-1}) which is absent in the UV-vis spectrum of the Mn^{II}-**3** complex. The decrease of the absorbance at 457 nm of Mn^{III}-**3** in the presence of excess ascorbic acid or BME, with the concomitant appearance of a new band characteristic of the Mn^{II}-**3** spectrum, was monitored over time. The experimental setup used to monitor the kinetics of the reaction consisted of a fiber coupled Ocean Optics spectrometer (USB4000-UV-Vis) used in absorption mode together with a MiKropack DH-2000-BAL UV-Vis-NIR light source. The absorption spectra were recorded in intervals of 50 ms (for ascorbic acid) and 100 ms (for BME) and monitored up to the complete formation of the Mn^{II}-**3** species. The large excess of ascorbic acid and of BME used in the experiments ensured pseudo-first-order kinetics with respect to the Mn^{III}-**3** complex as expressed in **equation (1)**:

$$\ln[\text{Mn}^{III}\text{-}\textbf{3}]_t = - k_{obs}\, t + \ln [\text{Mn}^{III}\text{-}\textbf{3}]_0 \qquad (1)$$

Here, k_{obs} refers to the observed pseudo-first-order rate constant, which is the product of the actual rate constant (k) and [ascorbic acid]$_0$, t is time and the subscripts "t" and "0" correspond to the calculated concentration at time "t" and the initial concentration, respectively.

Cyclic Voltammetry

The electrochemical experiments in aqueous solution were carried out using a 0.1 M HEPES buffer pH 7.4, prepared from N-[2-hydroxyethyl]piperazine-N´-[2-ethanesulfonic acid]) hemi sodium salt (Sigma, St. Louis, USA), as supporting electrolyte. The porphyrins stock solutions were prepared by dissolving the solid compounds in HEPES buffer, followed by further dilution in buffer when needed. Millipore Milli-Q nanopure water (resistivity ≥ 18 MΩ cm) was used for the preparation of all

solutions. All experiments were performed at room temperature (25 ± 1 ºC). The pH measurements were carried out with a CRISON 2001 micro pH-meter (Crison, Spain). The cyclic voltammetry (CV) measurements were carried out with an Autolab PGSTAT-30 potentiostat/galvanostat (Eco Chemie, Utrecht, Netherlands), controlled by GPES 4.9 software. The electrochemical cell, with a 2 mL volume, contained a glassy carbon electrode (d = 1mm) as working electrode, a platinum wire as counter and Ag/AgCl (3 M KCl) as reference electrode. Prior to the CV measurements, all solutions were degassed by N_2 bubbling for 15 min and during potential cycling a flux of N_2 was kept flowing on top of the cell solution.

Some CV measurements were also carried out in DCE solutions in the presence of 0.6 M Bu$_4$NBF$_4$. These were performed using a homemade potentiostat.[98] A jacketed five neck conical cell was used. Three of the necks were used for the working, counter, and reference electrodes, while the other two necks were used for the argon inlet and outlet. A glassy carbon disk with a 1 mm diameter was used as working electrode, with the counter electrode being a 1 mm diameter Pt disk. The reference electrode was a saturated calomel electrode (SCE), separated from the working electrode compartment by a salt bridge with a ceramic frit. Experiments were performed at 10 °C, using a HAAKE F3 circulation system in order to avoid the DCE solvent evaporation. Electrochemical characterisation of ferrocene was used as an electrochemical standard in DCE. Ferrocene showed a one-electron transfer. The current values were standardised with respect to concentration and scan rate square-root, in order to determine the number of electrons associated with an unknown electronic transfer.

All the potentials obtained were corrected to be reported referenced to the normal hydrogen electrode (NHE).

Cytotoxicity Studies

HeLa cells (human epithelial cervical carcinoma cell line) were maintained at 37 °C under an O_2/CO_2 (95%/5 %) atmosphere in Dulbecco's modified Eagle's medium (DMEM, Sigma, St. Louis, MO), supplemented with heat-inactivated fetal bovine serum (10 % (v/v), FBS, Sigma), penicillin (100 UmL^{-1}) and streptomycin (100 µgmL^{-1}). HeLa cells grown in monolayer were detached by treatment with trypsin solution (0.25 %, Sigma) and were seeded in medium (2×10^4 cells per mL (100 uL *per* well) in 96-well culture plates. After 24 h, when the cells were at 50–70 % confluence, they were incubated with the compound to be tested. The cytotoxicity induced by the compound in HeLa cells was evaluated using the modified Alamar Blue colorimetric assay, as previously described.[99] Briefly, a stock solution of the compound under study was prepared in phosphate buffer saline (PBS), and successive dilutions in DMEM complete medium were prepared from this stock in order to achieve the concentration range of 0.25 mM to 5 mM. The diluted solutions were added to the cells 24 h after seeding, followed by incubation of the cultures at 37 °C for 2, 4, and 24 h. For each time point, 0.1 mL of a resazurin dye solution (1% (v/v), Sigma) in DMEM medium was added to each well. After 45 min of incubation at 37 °C, the absorbance was measured at 570 and 600 nm with a SPECTRAmax PLUS 384 spectrophotometer

(Molecular Devices, Union City, CA). Although the compound under study is colored, its maximum absorbance is at $\lambda \approx 460$ nm and at $\lambda \approx 440$ nm, respectively for the oxidized and the reduced forms (**Figures 3 and S6**), thus not interfering with the results obtained from the Alamar Blue assay.

For each concentration of the compound, the percentage of cell viability was calculated according to **equation (2)**:

% cell viability = [(A$_{570}$ − A$_{600}$) treated cells / (A$_{570}$ − A$_{600}$) control cells] x 100   (2)

where the control cells (control +) refers to cells not exposed to the compound, corresponding to 100% of cell viability. It was also considered a negative control (control -) of the resazurin dye solution and the respective absorbance was subtracted to the values measured in all the samples.

Statistical analysis was carried out using one-way ANOVA with Tukey's multiple pairwise comparison. A value of $p < 0.05$ was considered as statistically significant

Conflicts of interest

There are no conflicts to declare.

Acknowledgements

Notes and references

1   1.   D. Trachootham, W. Q. Lu, M. A. Ogasawara, N. R. D. Valle and P. Huang, *Antioxid Redox Sign*, 2008, **10**, 1343-1374.

2   2.   D. F. Quail and J. A. Joyce, *Nat Med*, 2013, **19**, 1423-1437.

3   3.   N. W. Lutz, Y. Le Fur, J. Chiche, J. Pouyssegur and P. J. Cozzone, *Cancer Res*, 2013, **73**, 4616-4628.

4   4.   A. Rubartelli and M. T. Lotze, *Trends Immunol*, 2007, **28**, 429-436.

5   5.   E. H. Sarsour, M. G. Kumar, L. Chaudhuri, A. L. Kalen and P. C. Goswami, *Antioxid Redox Sign*, 2009, **11**, 2985-3011.

6   6.   D. J. Hausenloy and D. M. Yellon, *J Clin Invest*, 2013, **123**, 92-100.

7   7.   T. C. Jorgenson, W. X. Zhong and T. D. Oberley, *Cancer Res*, 2013, **73**, 6118-6123.

8   8.   R. Banerjee, *J Biol Chem*, 2012, **287**, 4397-4402.

9   9.   L. Chaiswing and T. D. Oberley, *Antioxid Redox Sign*, 2010, **13**, 449-465.

10   10.   F. Q. Schafer and G. R. Buettner, *Free Radical Bio Med*, 2001, **30**, 1191-1212.

11   11.   C. Vandeputte, I. Guizon, I. Genestiedenis, B. Vannier and G. Lorenzon, *Cell Biol Toxicol*, 1994, **10**, 415-421.

12   12.   I. Rahman, A. Kode and S. K. Biswas, *Nat Protoc*, 2006, **1**, 3159-3165.

13   13.   L. M. De Leon-Rodriguez, A. J. M. Lubag, C. R. Malloy, G. V. Martinez, R. J. Gillies and A. D. Sherry, *Accounts Chem Res*, 2009, **42**, 948-957.

14   14.   E. M. Gale, S. Mukherjee, C. Liu, G. S. Loving and P. Caravan, *Inorg Chem*, 2014, **53**, 10748-10761.

15   15.   M. Bourgeois, H. Rajerison, F. Guerard, M. Mougin-Degraef, J. Barbet, N. Michel, M. Cherel and A. Faivre-Chauvet, *Nuclear medicine review. Central & Eastern Europe*, 2011, **14**, 90-95.

16   16.   K. A. Wood, W. L. Wong and M. I. Saunders, *Nuclear medicine and biology*, 2008, **35**, 393-400.

17   17.   J. A. Alawneh, R. R. Moustafa, S. T. Marrapu, U. Jensen-Kondering, R. S. Morris, P. S. Jones, F. I. Aigbirhio, T. D. Fryer, T. A. Carpenter, E. A. Warburton and J. C. Baron, *European journal of nuclear medicine and molecular imaging*, 2014, **41**, 736-744.

18   18.   F. A. Rojas-Quijano, G. Tircso, E. T. Benyo, Z. Baranyai, H. T. Hoang, F. K. Kalman, P. K. Gulaka, V. D. Kodibagkar, S. Aime, Z. Kovacs and A. D. Sherry, *Chem-Eur J*, 2012, **18**, 9669-9676.

19   19.   K. Okuda, Y. Okabe, T. Kadonosono, T. Ueno, B. G. M. Youssif, S. Kizaka-Kondoh and H. Nagasawa, *Bioconjugate Chem*, 2012, **23**, 324-329.

20   20.   A. A. Bobko, T. D. Eubank, J. L. Voorhees, O. V. Efimova, I. A. Kirilyuk, S. Petryakov, D. G. Trofimiov, C. B. Marsh, J. L. Zweier, I. A. Grigor'ev, A. Samouilov and V. V. Khramtsov, *Magn Reson Med*, 2012, **67**, 1827-1836.

21   21.   P. Kuppusamy, H. Q. Li, G. Ilangovan, A. J. Cardounel, J. L. Zweier, K. Yamada, M. C. Krishna and J. B. Mitchell, *Cancer Res*, 2002, **62**, 307-312.

22   22.   Q. N. Do, J. S. Ratnakar, Z. Kovacs and A. D. Sherry, *ChemMedChem*, 2014, **9**, 1116-1129.

23   23.   E. L. Que and C. J. Chang, *Chem Soc Rev*, 2010, **39**, 51-60.

24   24.   P. B. Tsitovich, P. J. Burns, A. M. Mckay and J. R. Morrow, *J Inorg Biochem*, 2014, **133**, 143-154.

25   25.   D. V. Hingorani, A. S. Bernstein and M. D. Pagel, *Contrast Media Mol I*, 2015, **10**, 245-265.

26   26.   G. S. Loving, S. Mukherjee and P. Caravan, *J Am Chem Soc*, 2013, **135**, 4620-4623.

27   27.   C. Tu, R. Nagao and A. Y. Louie, *Angew Chem Int Edit*, 2009, **48**, 6547-6551.

28   28.   D. P. J. Pan, A. H. Schmieder, S. A. Wickline and G. M. Lanza, *Tetrahedron*, 2011, **67**, 8431-8444.

29   29.   E. M. Gale, I. P. Atanasova, F. Blasi, I. Ay and P. Caravan, *J Am Chem Soc*, 2015, **137**, 15548-15557.

30. E. M. Gale, C. M. Jones, I. Ramsay, C. T. Farrar and P. Caravan, *J Am Chem Soc*, 2016, **138**, 15861-15864.

31. E. Boros, E. M. Gale and P. Caravan, *Dalton T*, 2015, **44**, 4804-4818.

32. I. Bertini, C. Luchinat, G. Parigi and E. Ravera, *NMR of Paramagnetic Molecules - Applications to Metallobiomolecules and Models*, Elsevier, Amsterdam, 2017.

33. M. J. F. Calvete, S. M. A. Pinto, M. M. Pereira and C. F. G. C. Geraldes, *Coordin Chem Rev*, 2017, **333**, 82-107.

34. S. H. Koenig, R. D. Brown and M. Spiller, *Magn Reson Med*, 1987, **4**, 252-260.

35. N. Schaefle and R. Sharp, *J Phys Chem A*, 2005, **109**, 3267-3275.

36. R. Sharp, L. Lohr and J. Miller, *Prog Nucl Mag Res Sp*, 2001, **38**, 115-158.

37. D. Mansuy, *Cr Chim*, 2007, **10**, 392-413.

38. M. J. F. Calvete, M. Silva, M. M. Pereira and H. D. Burrows, *Rsc Adv*, 2013, **3**, 22774-22789.

39. C. A. Henriques, A. Fernandes, L. M. Rossi, M. F. Ribeiro, M. J. F. Calvete and M. M. Pereira, *Adv Funct Mater*, 2016, **26**, 3359-3368.

40. L. Cuesta-Aluja, J. Castilla, A. M. Masdeu-Bulto, C. A. Henriques, M. J. F. Calvete and M. M. Pereira, *J Mol Catal a-Chem*, 2016, **423**, 489-494.

41. D. Dini, M. J. F. Calvete and M. Hanack, *Chem Rev*, 2016, **116**, 13043-13233.

42. C. A. Henriques, S. M. A. Pinto, J. Pina, C. Serpa, A. Fernandes, L. M. Rossi, M. F. Ribeiro, M. M. Pereira and M. J. F. Calvete, *Dalton T*, 2016, **45**, 16211-16220.

43. A. T. Marques, S. M. A. Pinto, C. J. P. Monteiro, J. S. S. de Melo, H. D. Burrows, U. Scherf, M. J. F. Calvete and M. M. Pereira, *J Polym Sci Pol Chem*, 2012, **50**, 1408-1417.

44. S. M. A. Pinto, A. C. B. Neves, M. J. F. Calvete, A. R. Abreu, M. T. S. Rosado, T. Costa, H. D. Burrows and M. M. Pereira, *J. Photochem. Photobiol. A - Chem.*, 2012, **242**, 59-66.

45. A. V. C. Simoes, S. M. A. Pinto, M. J. F. Calvete, C. M. F. Gomes, N. C. Ferreira, M. Castelo-Branco, J. Llop, M. M. Pereira and A. J. Abrunhosa, *Rsc Adv*, 2015, **5**, 99540-99546.

46. M. J. F. Calvete, A. V. C. Simoes, C. A. Henriques, S. M. A. Pinto and M. M. Pereira, *Curr Org Synth*, 2014, **11**, 127-140.

47. S. M. A. Pinto, V. A. Tome, M. J. F. Calvete, M. M. Pereira, H. D. Burrows, A. M. S. Cardoso, A. Pallier, M. M. C. A. Castro, E. Toth and C. F. G. C. Geraldes, *J Inorg Biochem*, 2016, **154**, 50-59.

48. A. V. C. Simoes, A. Adamowicz, J. M. Dabrowski, M. J. F. Calvete, A. R. Abreu, G. Stochel, L. G. Arnaut and M. M. Pereira, *Tetrahedron*, 2012, **68**, 8767-8772.

49. D. J. Todd and J. Kay, *Annu Rev Med*, 2016, **67**, 273-291.

50. M. Aschner, T. R. Guilarte, J. S. Schneider and W. Zheng, *Toxicol Appl Pharm*, 2007, **221**, 131-147.

51. L. J. Jing, X. L. Liang, X. D. Li, Y. B. Yang and Z. F. Dai, *Acta Biomater.*, 2013, **9**, 9434-9441.

52. T. J. Zou, M. M. Zhen, D. Q. Chen, R. M. Li, M. R. Guan, C. Y. Shu, H. B. Han and C. R. Wang, *Dalton T*, 2015, **44**, 9114-9119.

53. W. R. Cheng, I. E. Haedicke, J. Nofiele, F. Martinez, K. Beera, T. J. Scholl, H. L. M. Cheng and X. A. Zhang, *J Med Chem*, 2014, **57**, 516-520.

54. T. D. MacDonald, T. W. Liu and G. Zheng, *Angew Chem Int Edit*, 2014, **53**, 6956-6959.

55. G. G. Westmeyer, Y. Emer, J. Lintelmann and A. Jasanoff, *Chem Biol*, 2014, **21**, 422-429.

56. I. E. Haedicke, T. Li, Y. L. K. Zhu, F. Martinez, A. M. Hamilton, D. H. Murrell, J. T. Nofiele, H. L. M. Cheng, T. J. Scholl, P. J. Foster and X. A. Zhang, *Chem Sci*, 2016, **7**, 4308-4317.

57. X. A. Zhang, K. S. Lovejoy, A. Jasanoff and S. J. Lippard, *Proc. Natl. Acad. Sci. USA*, 2007, **104**, 10780-10785.

58. T. Lee, X. A. Zhang, S. Dhar, H. Faas, S. J. Lippard and A. Jasanoff, *Chem Biol*, 2010, **17**, 665-673.

59. S. Aime, M. Botta, E. Gianolio and E. Terreno, *Angew Chem Int Edit*, 2000, **39**, 747-750.

60. M. Silva, A. Fernandes, S. S. Bebiano, M. J. F. Calvete, M. F. Ribeiro, H. D. Burrows and M. M. Pereira, *Chem Commun*, 2014, **50**, 6571-6573.

61. G. R. Friedermann, M. Halma, K. A. Dias de Freitas Castro, F. L. Benedito, F. G. Doro, S. M. Drechsel, A. S. Mangrich, M. D. Assis and S. Nakagaki, *Appl Catal a-Gen*, 2006, **308**, 172-181.

62. Q. Yu, Y. H. Liu, D. S. Liu and J. F. Li, *Dalton T*, 2015, **44**, 9382-9390.

63. P. Turner and M. J. Gunter, *Inorg Chem*, 1994, **33**, 1406-1415.

64. W. Harhouri, S. Dhifaoui, Z. Denden, T. Roisnel, F. Blanchard and H. Nasri, *Polyhedron*, 2017, **130**, 127-135.

65. R. Guilard, K. Perie, J. M. Barbe, D. J. Nurco, K. M. Smith, E. Van Caemelbecke and K. M. Kadish, *Inorg Chem*, 1998, **37**, 973-981.

66. M. A. C. deMedeiros, S. Cosnier, A. Deronzier and J. C. Moutet, *Inorg Chem*, 1996, **35**, 2659-2664.

67. E. J. Sun, Y. H. Shi, P. Zhang, M. Zhou, Y. H. Zhang, X. X. Tang and T. S. Shi, *J Mol Struct*, 2008, **889**, 28-34.

68. L. Ruhlmann, A. Nakamura, J. G. Vos and J. H. Fuhrhop, *Inorg Chem*, 1998, **37**, 6052-6059.

69. F. C. Chen, S. H. Cheng, C. H. Yu, M. H. Liu and Y. O. Su, *J Electroanal Chem*, 1999, **474**, 52-59.

70. M. A. Luna, F. Moyano, L. Sereno and F. D'Eramo, *Electrochim Acta*, 2014, **135**, 301-310.

71. S. Romain, C. Duboc, F. Neese, E. Riviere, L. R. Hanton, A. G. Blackman, C. Philouze, J. C. Lepretre, A. Deronzier and M. N. Collomb, *Chem-Eur J*, 2009, **15**, 980-988.

72. X. Q. Jiang, C. P. Gros, Y. Chang, N. Desbois, L. H. Zeng, Y. Cui and K. M. Kadish, *Inorg Chem*, 2017, **56**, 8045-8057.

73   73.   A. Harriman, *J Chem Soc Dalton*, 1984, DOI: Doi 10.1039/Dt9840000141, 141-146.

74   74.   A. J. Bard, *Journal*, 2001.

75   75.   S. E. Creager and R. W. Murray, *Inorg Chem*, 1987, **26**, 2612-2618.

76   76.   J. A. Hodge, M. G. Hill and H. B. Gray, *Inorg Chem*, 1995, **34**, 809-812.

77   77.   L. J. Boucher, *Coordin Chem Rev*, 1972, **7**, 289-329.

78   78.   S. L. H. Rebelo, M. M. Pereira, M. M. Q. Simoes, M. G. P. M. S. Neves and J. A. S. Cavaleiro, *J Catal*, 2005, **234**, 76-87.

79   79.   E. Vancaemelbecke, W. Kutner and K. M. Kadish, *Inorg Chem*, 1993, **32**, 438-444.

80   80.   L. Robitaille and L. J. Hoffer, *Nutr J*, 2016, **15**.

81   81.   M. Levine, C. ConryCantilena, Y. H. Wang, R. W. Welch, P. W. Washko, K. R. Dhariwal, J. B. Park, A. Lazarev, J. F. Graumlich, J. King and L. R. Cantilena, *Proc. Natl. Acad. Sci. USA*, 1996, **93**, 3704-3709.

82   82.   Y. I. Turyan and R. Kohen, *J Electroanal Chem*, 1995, **380**, 273-277.

83   83.   C. E. Aitken, R. A. Marshall and J. D. Puglisi, *Biophys J*, 2008, **94**, 1826-1835.

84   84.   L. H. Bryant, M. W. Hodges and R. G. Bryant, *Inorg Chem*, 1999, **38**, 1002-1005.

85   85.   M. M. Williamson and C. L. Hill, *Inorg Chem*, 1987, **26**, 4155-4160.

86   86.   D. Lieb, A. Zahl, T. E. Shubina and I. Ivanovic-Burmazovic, *J Am Chem Soc*, 2010, **132**, 7282-7284.

87   87.   A. Budimir, K. Jozsef, F. Istvan, G. Lente, B. Istvan, I. Batinic-Haberle and M. Birus, *Dalton T*, 2010, **39**, 4405-4410.

88   88.   J. K. Moscicki, Y. K. Shin and J. H. Freed, *J Chem Phys*, 1993, **99**, 634-649.

89   89.   B. Drahos, J. Kotek, P. Hermann, I. Lukes and E. Toth, *Inorg Chem*, 2010, **49**, 3224-3238.

90   90.   Y. Ducommun, K. E. Newman and A. E. Merbach, *Inorg Chem*, 1980, **19**, 3696-3703.

91   91.   I. Bertini, F. Briganti, Z. C. Xia and C. Luchinat, *J Magn Reson Ser A*, 1993, **101**, 198-201.

92   92.   A. Sour, S. Jenni, A. Orti-Suarez, J. Schmitt, V. Heitz, F. Bolze, P. L. de Sousa, C. Po, C. S. Bonnet, A. Pallier, E. Toth and B. Ventura, *Inorg Chem*, 2016, **55**, 4545-4554.

93   93.   K. H. Chalmers, E. De Luca, N. H. M. Hogg, A. M. Kenwright, I. Kuprov, D. Parker, M. Botta, J. I. Wilson and A. M. Blamire, *Chem-Eur J*, 2010, **16**, 134-148.

94   94.   S. R. Davis, E. P. Quinlivan, P. W. Stacpoole and J. F. Gregory, *J Nutr*, 2006, **136**, 373-378.

95   95.   K. P. Malikidogo, I. Da Silva, J. F. Morfin, S. Lacerda, L. Barantin, T. Sauvage, J. Sobilo, S. Lerondel, E. Toth and C. S. Bonnet, *Chem Commun*, 2018, **54**, 7597-7600.

96   96.   S. A. Graves, R. Hemandez, J. Fonslet, C. G. England, H. F. Valdovinos, P. A. Ellison, T. E. Barnhart, D. R. Elema, C. P. Theuer, W. B. Cai, R. J. Nickles and G. W. Severin, *Bioconjugate Chemistry*, 2015, **26**, 2118-2124.

97   97.   A. M. D. R. Gonsalves, R. A. W. Johnstone, M. M. Pereira, A. M. P. deSantAna, A. C. Serra, A. J. F. N. Sobral and P. A. Stocks, *Heterocycles*, 1996, **43**, 829-838.

98   98.   D. Garreau and J. M. Saveant, *J Electroanal Chem*, 1972, **35**, 309-&.

99   99.   A. M. S. Cardoso, H. Faneca, J. A. S. Almeida, A. A. C. C. Pais, E. F. Marques, M. C. P. de Lima and A. S. Jurado, *BBA-Biomembranes*, 2011, **1808**, 341-351.

100